Supporting Information

Zn(II)-Doped Cesium Lead Halide Perovskite Nanocrystals with High Quantum Yield and Wide Color Tunability for Color-Conversion Light-Emiting Diodes

V. Naresh [†]*, and Nohyun Lee* [*,†]

[†]School of Advanced material Engineering, Kookmin University, Seoul 02707, and Republic of Korea.

*Corresponding author email: nohyunlee@kookmin.ac.kr (Nohyun Lee)

Materials and chemicals:

Lead chloride ($PbCl_2$, 99.99% Sigma-Aldrich), caesium carbonate (Cs_2CO_3, 99.99% Sigma-Aldrich), zinc chloride hydrate ($ZnCl_2$ H_2O, 99.99% Sigma-Aldrich), zinc acetate ($ZnC_4H_6O_4$ or $Zn(Ac)_2$, 99.99% Sigma-Aldrich)1-octadecene (ODE, 90% Sigma-Aldrich), oleic acid (OA, 90% Sigma-Aldrich), oleylamine (OLA, 80-90% Sigma-Aldrich), Methyl acetate (MeOAc, 99.5% Sigma-Aldrich), Trioctylphosphine (TOP, 90% Sigma-Aldrich), trimethylchlorosilane (TMS-Cl, 99% Sigma-Aldrich), n-hexane (95.0% Samchun), toluene (99.99% Samchun) and Poly(methyl methacrylate) (PMMA, Mw: ~350,000 by GPC, Sigma-Aldrich) were purchased and used without further purification.

Synthesis methodology:

Preparation of caesium-oleate: Cs_2CO_3 (0.4073 g, 1.25 mmol), 15 mL ODE and 1.35 mL OA were loaded into a 100 mL 3-neck flask, heated to 120 °C under vacuum for 1 h, and then heated under Ar gas flow at 150 °C until Cs_2CO_3 was completely dissolved, and a clear solution was obtained. The Cs-oleate solution is kept at this temperature (150 °C) before it was injected.

Synthesis of $CsPbCl_3$ perovskite NCs: $PbCl_2$ (0.104 g, 0.376 mmol) and ODE (10 mL) were loaded into a 50 mL 3-neck flask, heated to 120 °C under vacuum for 1 hr, and then followed by heating the solution to 150 °C under Ar gas. At this temperature, 2 mL TOP was swiftly injected and stirred until $PbCl_2$ salt was completely dissolved. After raising the temperature to 180 °C, OLA (1 mL) and OA (1 mL) dried at 100 °C for 1 h were subsequently injected into the PbX_2-ODE solution in the flask under the flow of Ar gas. After complete solubilization, the temperature was raised to 190 °C and kept at this temperature for 5 minutes. Then, Cs-oleate solution (0.9 mL, 0.15M in ODE) was quickly injected into the PbX_2-ODE solution and after 60 s the solution was immediately cooled down to room temperature by immersing the flask in an ice-water bath.

Synthesis of Zn-doped $CsPbCl_3$ and Zn-doped $CsPb(Cl/Br)_3$ perovskite NCs. The procedure described above was followed for the synthesis of $CsPbCl_3$: Zn and $CsPb(Cl/Br)_3$: Zn PNCs. A specific amount of $PbCl_2$ and $ZnCl_2$ (feed ratio of $ZnCl_2$ to $PbCl_2$ are 0, 0.5, 1, 1.5, 2.0) and ODE (10 mL) were loaded into a 50 mL 3-neck flask and heated to 120 °C under vacuum for 1 h and then followed by heating the solution to 150 °C under Ar gas. At this temperature, 2 mL TOP was swiftly injected and stirred until $PbCl_2$ and $ZnCl_2$ salts were completely dissolved and the solution becomes clear. Then, the temperature was raised to 200 °C, OLA (1 mL) and OA (1 mL) dried at 100 °C for 1 h were subsequently injected into the PbX_2-ODE solution in the flask under the flow of Ar gas. After complete solubilization, the temperature was raised to 210 °C and kept at this temperature for 5 minutes. Then, Cs-oleate solution (0.9 mL, 0.15M) was quickly injected into the PbX_2-ODE solution and after 60 s the solution was immediately cooled down to room temperature by immersing the flask in an ice-water bath. For $CsPb(Cl/Br)_3$: Zn PNCs synthesis, a certain amount of $PbCl_2$ (0.188 mmol), $ZnCl_2$, $PbBr_2$ (0.188 mmol) and ODE (10 mL) were taken into 100 mL 3-neck flask, and above described synthesis procedure was followed.

Synthesis of $Zn(Ac)_2$ and TMS-Cl doped $CsPbCl_3$ perovskite NCs. ODE (10 ml), $PbCl_2$ and Zn(Ac)2 in 1: 1 feed ratio and TMS-Cl (1 mmol) were taken into 50 ml 3-neck flask, heated to 120 °C under vacuum for 1 h to dissolve the precursors and remove water, and then followed by heating the solution to 150 °C under Ar gas. The temperature was raised 180 °C, OLA (2 mL) and OA (2 mL) dried at 100 °C for 1 h were subsequently injected into the PbX_2-ODE solution in the flask under the flow of Ar gas. After complete solubilization, the temperature was raised to 200 °C and kept at this temperature for 5 minutes. Then, Cs-oleate solution (0.9 mL, 0.15M in ODE) was quickly injected into the PbX_2-ODE solution and after 60 s the solution was immediately cooled down to room temperature by immersing the flask in an ice-water bath. Similar procedure was repeated by varying TMS-Cl from 0.5 to 3 mmol for the fixed concentration of $Zn(Ac)_2$ (1 mmol) and for the varied concentration of $Zn(Ac)_2$ from 0.5 to 3 mmol keeping TMS-Cl fixed to 1 mmol.

Purification of nanocrystals. As-synthesized $CsPbCl_3$, Zn-doped $CsPbCl_3$ and Zn-doped $CsPb(Cl/Br)_3$ PNCs were extracted from the crude solution by centrifuging at 8000 rpm for 5 min and then discard the supernatant. This process was repeated for one more time by adding 4 ml MeOAc and centrifuged to remove the residual mixture. Then, the precipitate was redispersed in 2 ml MeOAc and 2 ml n-hexane and centrifuged again for 5 min at 8000 rpm, and the supernatant was discarded. Subsequently, the particles in the centrifuge tube were dispersed again in 5 ml n-hexane and centrifuged for 5 min at 5000 rpm supernatant was discarded. Finally, the precipitate was re-dispersed in toluene (or n-hexane for optical characterization) forming stable colloidal solutions. For solid NCs powders, the precipitate obtained in the above step was dried under vacuum at 60 °C overnight.

Synthesis of $CsPbBr_3$ and $CsPb(Br/I)_3$ perovskite NCs. As described above, for the synthesis of $CsPbBr_3$ PNCs, $PbBr_2$ (0.188 mmol; 0.069 g) and for the synthesis of $CsPb(Br/I)_3$, $PbBr_2$ (0.069 g) and PbI_2 (0.087 g) were added into a 50 mL three-necked flask containing 5 mL of ODE and heated at 120 °C for 1 h under vacuum. Dried OLA (0.5 mL) and OA (0.5 mL) at 100 °C for 1 hr were injected into the PbX_2-ODE solution at 120 °C under Ar flow. After the solution turned clear, the temperature was raised to 140–160 °C and the Cs-oleate solution (0.4 mL) was quickly injected into the PbX_2-ODE solution, and 30 s later, the reaction mixture was cooled by an ice-water bath. As the synthesized solution was purified by centrifuging for 5 min at 8000 rpm and the supernatant was discarded and the process is repeated for a couple of times. Subsequently, the particles in the centrifuge tube were dispersed again in 5 ml of toluene.

Preparation of PNCs@PMMA blended solid films. A mixture of 1 g PMMA powder (M_w ~ 350, 000) and 10 ml toluene were taken into 25 ml flask and stirred vigorously at 80 °C (overnight) until the PMMA powder dissolves completely and the solution becomes transparent and colourless. The $CsPb(Cl/Br)_3$:Zn, $CsPbBr_3$ and $CsPb(Br/I)_3$ PNCs were separately dispersed in PMMA solution and stirred vigorously to obtain homogeneously dispersed NCs in PMMA solution blend. Thus, the resultant solution blend was drop-casted on a silica glass slide and dried in a vacuum chamber to remove the solvent. Finally, NCs blended solid PMMA films were obtained (PNCs@PMMA).

Designing of PNCs@PMMA coated LED devise. The prepared PNCs@PMMA can produce blue (Zn-doped $CsPb(Cl/Br)_3$), green ($CsPbBr_3$ NCs) and red ($CsPbBr_3$ NCs) emissions individually. A prototype white-LED device is fabricated by directly stacking the

PNCs solid films of $CsPb(Cl/Br)_3$:Zn @PMMA/glass, $CsPbBr_3$ NCs @PMMA/glass, and $CsPb(Br/I)_3$ NCs @PMMA/glass one over the other and finally coupled on to a commercially available 365 nm UV-LED chip (as shown in Figure 9a). To avoid the leakage of the light, the edges of the glass slide are wrapped with black tape.

Characterizations.

XRD patterns were recorded on a Bruker DE/D8 Advance X-ray Diffractometer equipped with Cu Kα (λ = 1.541 Å) radiation source operated at 60kV and 60 mA at room temperature. The samples were provided in dry powder form and scanned within the range of 2θ from 10 to 60°. The morphology of the pristine and Zn-doped perovskite nanocrystals was investigated from the transmission electron microscopy (TEM) and high-resolution TEM (HR-TEM) images acquired on a JEM-2100/ JEOL/ JP operated at 200 kV accelerating voltage. The 300 mesh copper Formvar/ carbon grid was dipped into the PNCs dispersed toluene solution and allowed to dry in ambient conditions overnight. Inductively coupled plasma-atomic emission spectroscopy (ICP-AES) characterization was carried out on a Shimadzu ICPS-8100 twin sequential high-frequency plasma emission spectrometer. The dried PNCs were first digested in warm (1% HNO_3 and 1% HCl) acid solution (~70 °C, 6-8 hours) until completely dissolved forming a transparent liquid. The obtained solution was then diluted with deionized water, and the resultant solution was filtered through a syringe filter with 0.22 μm pore size before the analysis. The thermos-gravimetric analysis (TGA: mass) and differential thermal analysis (DTA: temperature) were simultaneously measured for PNCs by employing the NETZSCH STA 449F5 instrument. The samples were measured under an N_2 atmosphere as a purging gas, ranging from 30°C to 1000 °C with a heating rate of 10 K/min. The X-ray photoelectron spectroscopy (XPS) measurement was conducted on an Ulvac PHI/X-tool spectrometer with Al Kα radiation source (1486.6 eV, 24.1W, 15kV) and a beam diameter of 100μm*100μm. UV-Vis absorption spectra were measured in the range of 300-700 nm on a Shimadzu UV-2600 spectrometer. The $CsPbCl_3$ and Zn-doped $CsPbCl_3$ NCs dispersed in toluene were used for the absorption, PL and time-resolved spectroscopy measurements. The steady-state fluorescence spectra (PL and PLE) were recorded using a Shimadzu RF-6000 Spectro-fluoro-photometer equipped with a 150 W Xe lamp as an excitation and scanning speed 60,000 nm/min. The time-resolved decay curves of the samples were measured on a HORIBA Jobin Yvon FluoroMax-4 fluorescence spectrometer equipped with a 150 W Xe lamp as an excitation source at room temperature. The PLQY of the PNCs dispersed toluene solutions were measured by employing an integrated sphere unit attached to Shimadzu RF-6000 Spectro-fluoro-photometer according to the standard procedure using Toluene as a reference under ambient conditions. Electroluminescence spectra were measured on Labsphere CdS-610 spectrometer. The temperature stability test was carried by depositing pristine and Zn-doped $CsPbCl_3$ PNCs onto a glass slide and heated at different temperatures (from room temperature to 413 K) under ambient conditions. The effect of moisture (water-stability test) on the pristine and Zn-doped PNCs was evaluated by soaking 2.5 mL of PNCs solution in 2.5 mL of deionized water for 24 h. The Photo-stability measurement was carried for pristine and Zn-doped $CsPbCl_3$ PNCs solutions by continuous irradiating with a UV lamp (365 nm, 6W) placed at a distance of 1 cm for 78 hr.

Table S1. ICP-AES data analysis of $CsPbCl_3$:*x*%Zn PNCs with different concentrations of Zn

Feed ratio $ZnCl_2$:$PbCl_2$	Pb concentration [ppm]	Zn concentration [ppm]	Pb ratio (%)	Zn ratio (%)	composition
0	330.5	0	100	0	$CsPbCl_3$
0.5:1	216.3	4.99	97.74	2.3	$CsPb_{0.93}Zn_{0.07}Cl_3$
1:1	293	18.07	94.19	5.8	$CsPb_{0.84}Zn_{0.16}Cl_3$
1.5:1	268.2	25.32	91.37	8.6	$CsPb_{0.77}Zn_{0.23}Cl_3$
2:1	253.3	33.12	88.43	11.6	$CsPb_{0.71}Zn_{0.29}Cl_3$

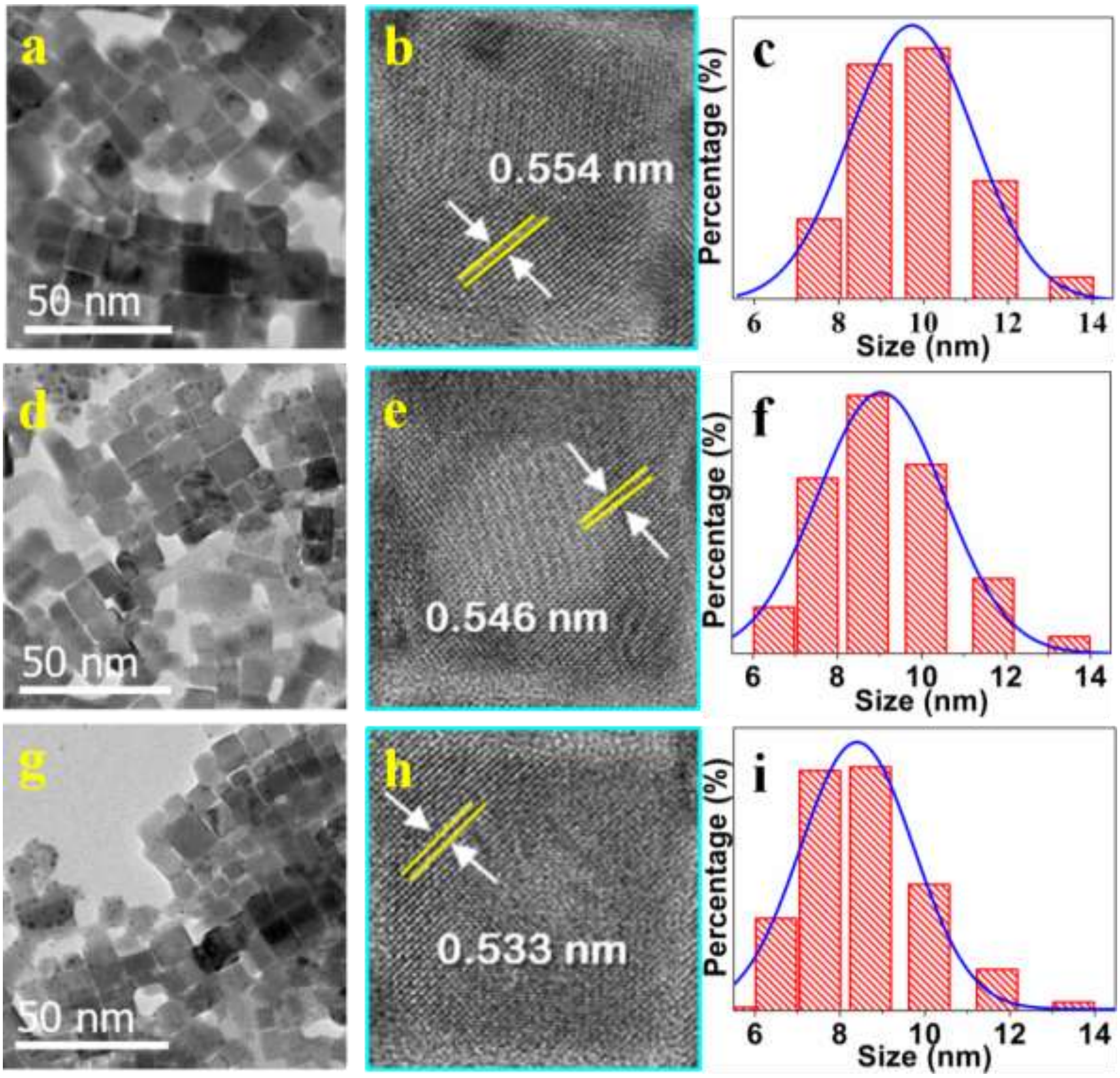

Figure S1. TEM, HR-TEM images and their corresponding particle distribution histograms displaying size and shape of $CsPbCl_3$: 2.3% Zn (a, b and c), $CsPbCl_3$: 5.8% Zn (d, e, and f) and $CsPbCl_3$: 11.6% Zn (g, h, and i) PNCs, respectively.

Table S2. Sample composition, 2θ values, lattice constant of $CsPbCl_3$ and Zn-doped $CsPbCl_3$ PNCs.

Sample	**Peak (110) position 2 θ (degrees)**	**Lattice constant (Å) (±0.01)**	**Avg edge length (nm)**
$CsPbCl_3$	22.43	0.564	10.13
$CsPbCl_3$: 2.3% Zn	22.47	0.559	9.73
$CsPbCl_3$: 5.8% Zn	22.51	0.558	9.04
$CsPbCl_3$: 8.6% Zn	22.56	0.557	8.72
$CsPbCl_3$: 11.6% Zn	22.59	0.556	8.40

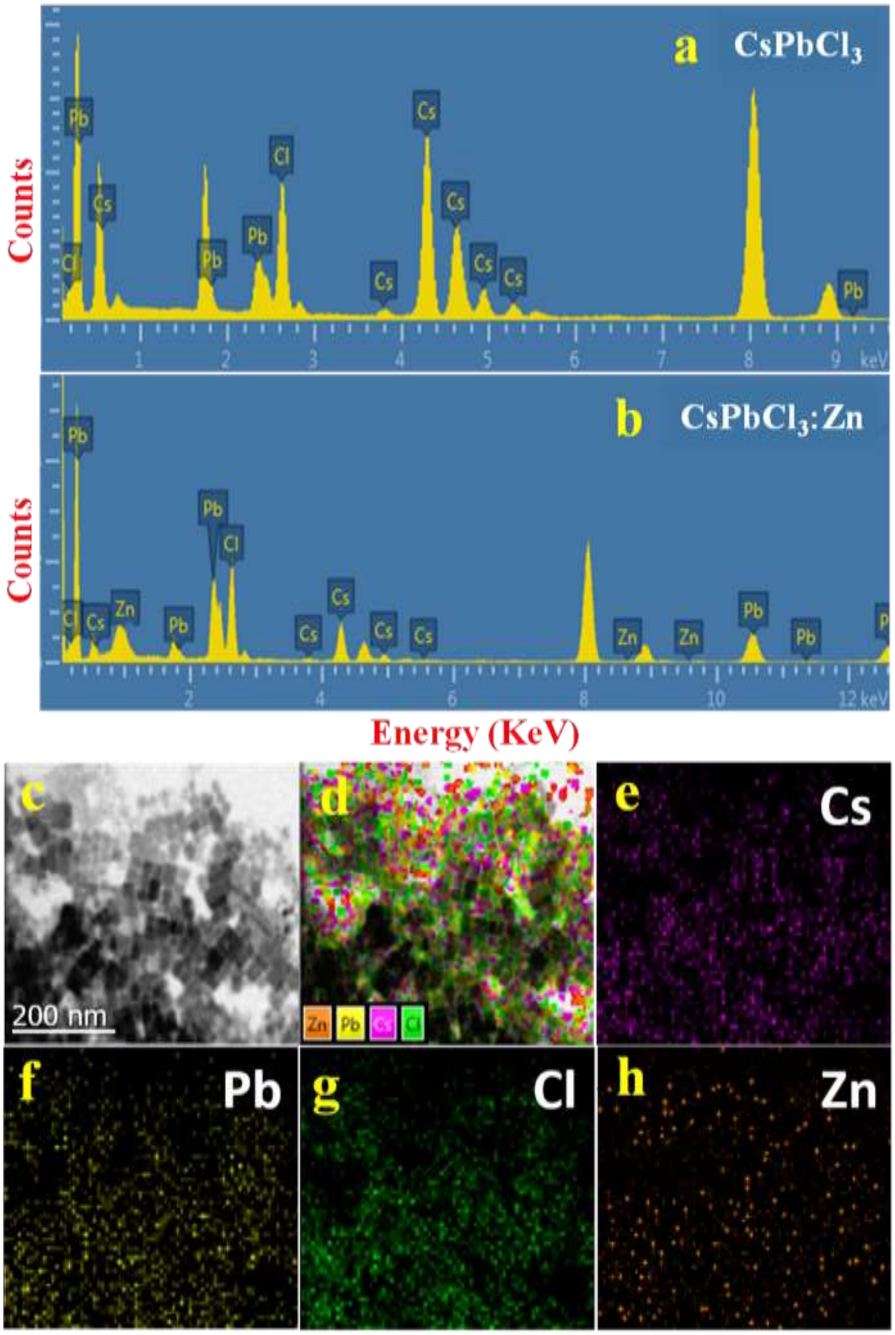

Figure S2. Elemental signal (EDS) profiles of (a) $CsPbCl_3$, (b) $CsPbCl_3$:Zn and (c-h) elemental composition (mapping) images Cs, Pb, Cl and Zn in $CsPbCl_3$:Zn PNCs.

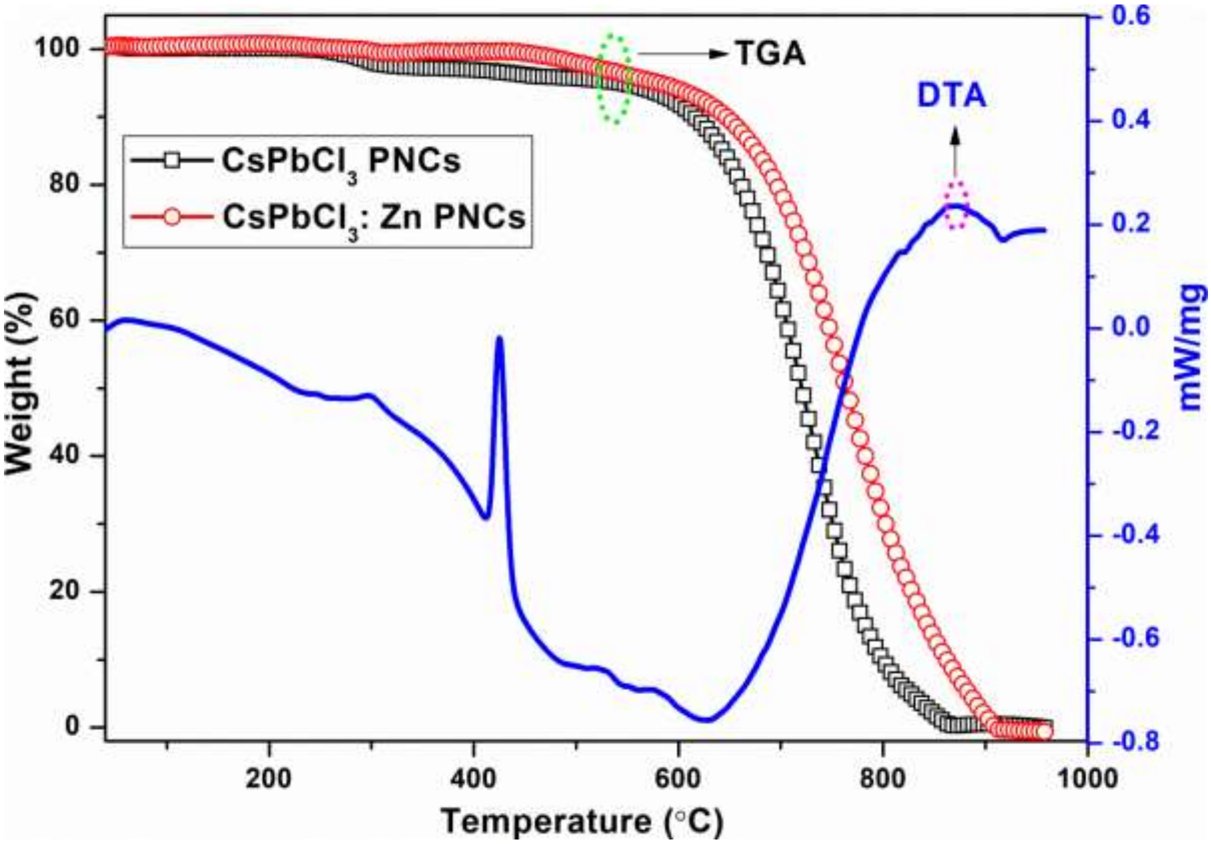

Figure S3. TGA-DTA profiles of pristine $CsPbCl_3$ and Zn-doped $CsPbCl_3$ PNCs.

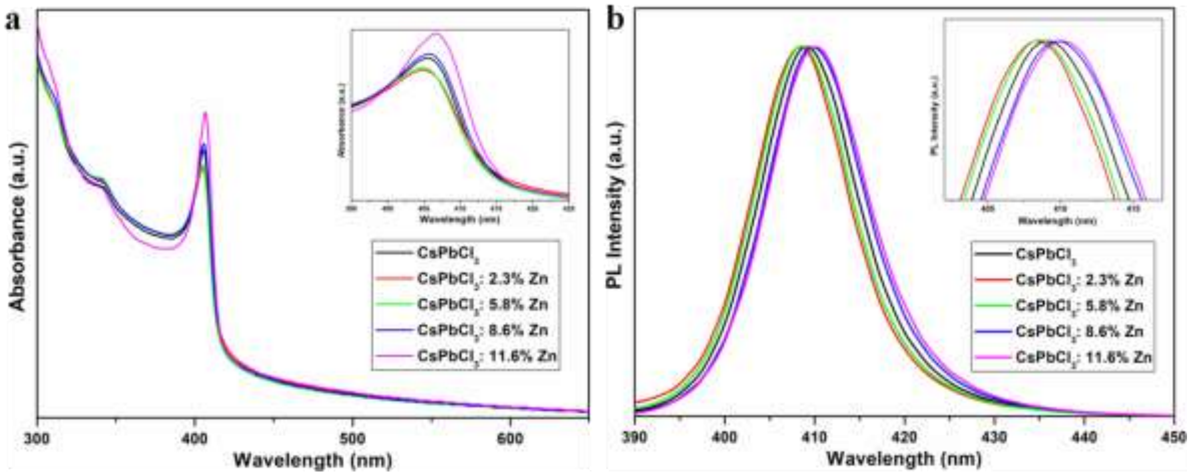

Figure S4. (a) Normalized optical absorption and (b) normalized photoluminescence spectra of parent $CsPbCl_3$ and $CsPbCl_3$: *x*% Zn (*x* = 2.3, 5.8, 8.6, and 11.6%) PNCs.

Table S3. Average lifetimes τ_{avg} of fitted PL decay curves, PLQYs, radiative (τ_r) and non-radiative (τ_{nr}) decay rates of $CsPbCl_3$ and $CsPbCl_3$: *x*% Zn (*x* = 2.3, 5.8, 8.6, and 11.6%) PNCs

Sample	τ_1 **(ns)**	**A1**	τ_2 **(ns)**	**A2**	τ_3 **(ns)**	**A3**	τ_{avg} **(ns)**	**PLQY (%)**	τ_r **(ns^{-1})**	τ_{nr} **(ns^{-1})**
$CsPbCl_3$	0.165	0.62	0.55	0.42	3.35	0.046	1.35	3.2	0.023	0.71
$CsPbCl_3$: 2.3% Zn	0.45	0.48	0.30	0.32	4.94	0.051	2.40	16	0.057	0.35
$CsPbCl_3$: 5.8% Zn	0.35	0.53	1.35	0.36	5.81	0.076	2.95	38	0.128	0.21
$CsPbCl_3$: 8.6% Zn	0.33	0.62	1.53	0.42	9.45	0.063	4.62	88.7	0.191	0.025
$CsPbCl_3$: 11.6% Zn	0.51	0.63	2.15	0.57	8.02	0092	3.86	73	0.18	0.069

, where $\tau_{avg} = {\sum a_i \tau_i^2}/{a_i \tau_i}$, $\tau_r = {PLQY(\%)}/{\tau_{avg}}$, $\tau_{nr} = {1 - PLQY(\%)}/{\tau_{avg}}$.

Table S4. The PLQY of our Zn-doped $CsPbCl_3$ PNCs is compared with the reported values of the divalent metal cation doped $CsPbCl_3$ PNCs

Sample	PLQY (%)	Method	References
Ni^{2+}- doped $CsPbCl_3$	96.5	Hot-Injection	Ref. 1
Cd^{2+}- doped $CsPbCl_3$	96-98	Post-synthetic	Ref. 2
Ca^{2+}- doped $CsPbCl_3$	77.1	Hot-Injection	Ref. 3
Cu^{2+}- doped $CsPbCl_3$	60	Hot-Injection	Ref. 4
Fe^{3+}- doped $CsPbCl_3$	4.32	Hot-Injection	Ref. 5
Zn^{2+}- doped $CsPbCl_3$	88.7	Hot-Injection	(present work)

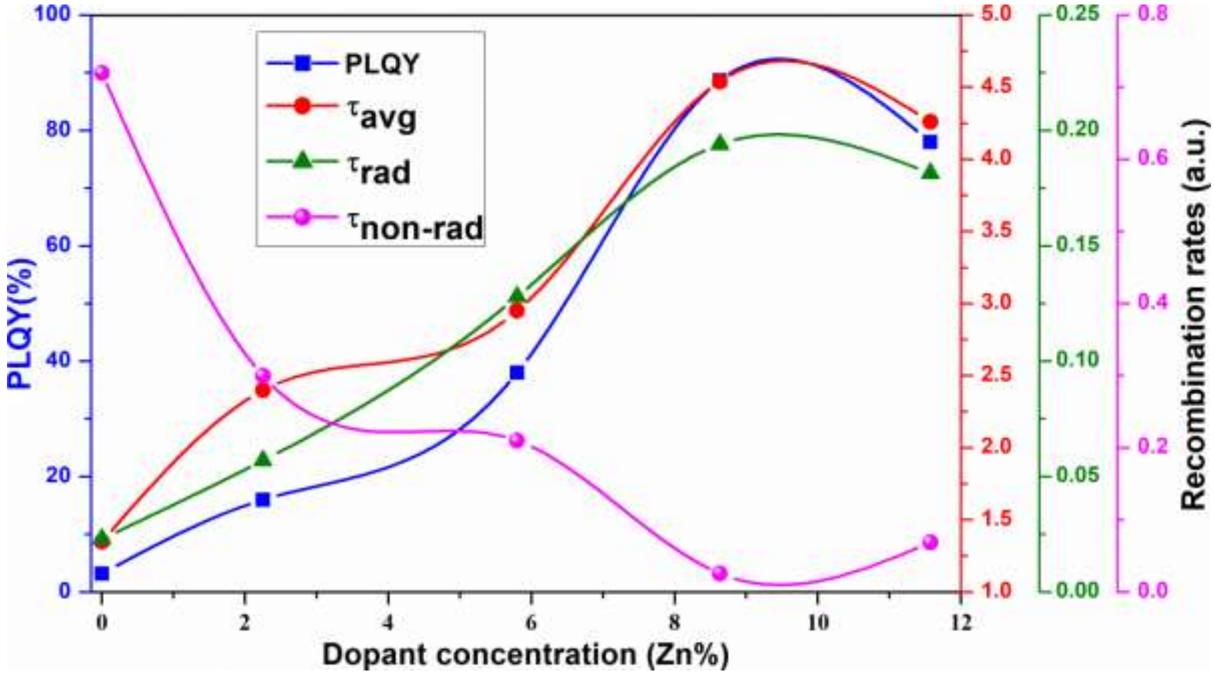

Figure S5. Average lifetime, PLQY, recombination rates (radiative and non-radiative) as a function of dopant (Zn%) ion concentration.

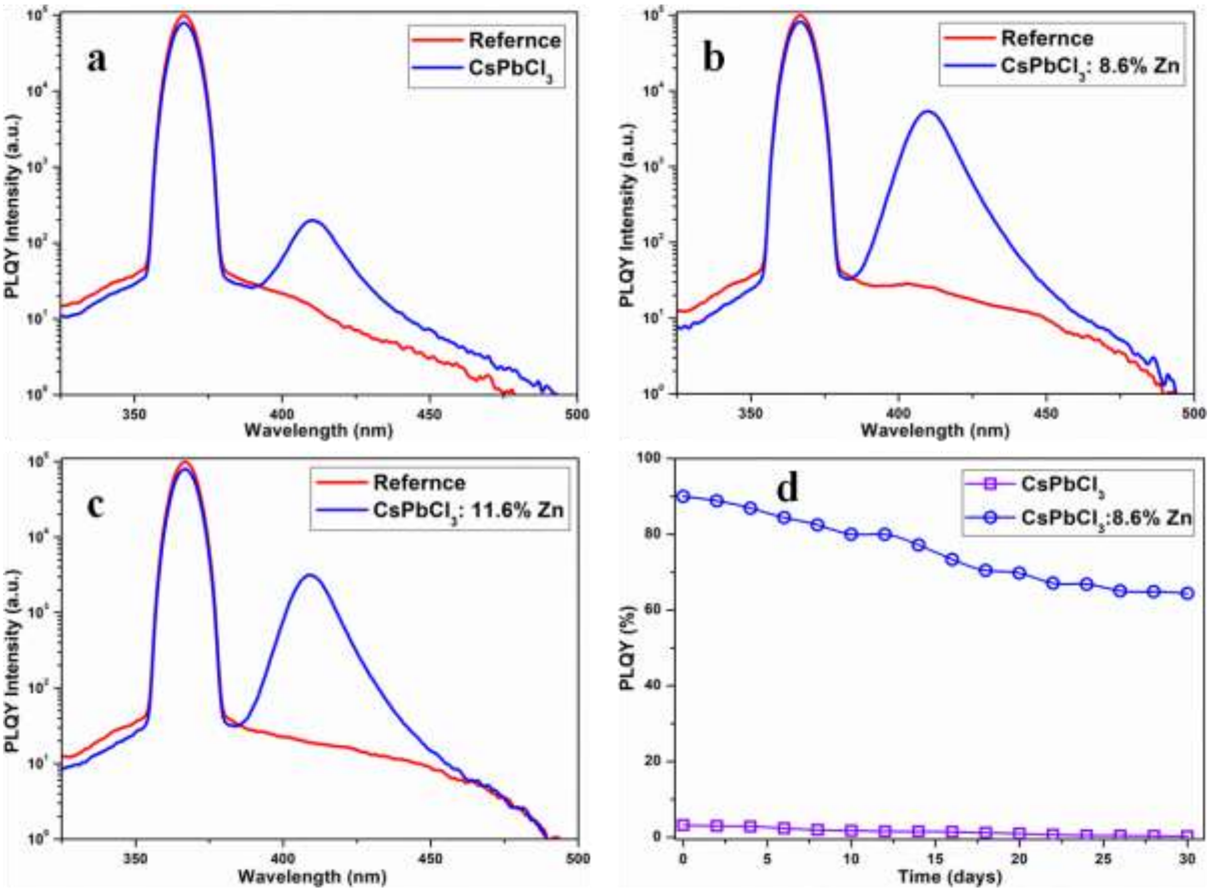

Figure S6. PLQY measurement of (a) $CsPbCl_3$, (b) $CsPbCl_3$:8.6%Zn, (c) $CsPbCl_3$:11.6%Zn PNCs, and (d) PLQY of $CsPbCl_3$ and $CsPbCl_3$:8.6%Zn PNCs under ambient conditions for 30 days.

Investigation on suppresssion of vacancies and disorder via incorporation of Zn^{2+} and Cl^{-} ($Zn(Ac)_2$ and TMS-Cl as Zn^{2+} and Cl^{-} source) in $CsPbCl_3$ PNCs

To evaluate the exchange mechanism between Zn^{2+} and Pb^{2+} cations in suppressing the formation of chlorine vacancies and strain relaxation without introducing defect states (traps), we extended the experimental study to examine the doping behavior of Zn ion (in the form of Zinc acetate; $Zn(Ac)_2$) via cation exchange route and Cl^{-} ion (in the form of trimethylchlorosilane; TMS-Cl) through Cl-Cl exchange. The PL features of the pristine PNCs are compared with Zn acetate doped $CsPbCl_3$, TMS-Cl doped $CsPbCl_3$ and (Zn acetate and TMS-Cl) combinedly doped $CsPbCl_3$ PNCs shown in Figure S7a.

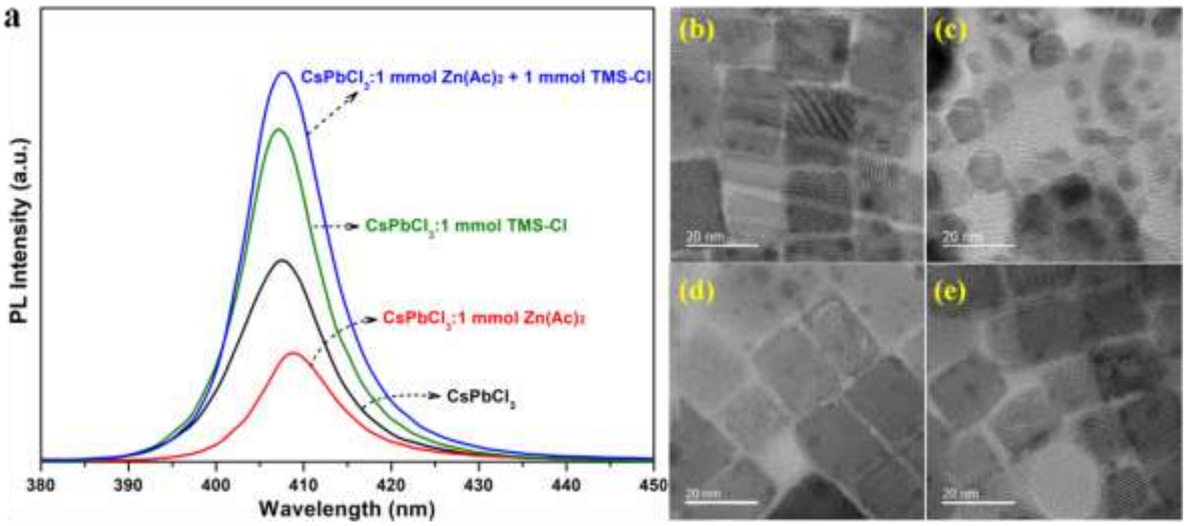

Figure S7. (a) shows the emission profiles of pristine $CsPbCl_3$, Zn^{2+} added ($Zn(Ac)_2$ as Zn source), TMS-Cl added (triethylchlorosilane as Cl source) and both ($Zn(Ac)_2$ +TMS-Cl) co-added $CsPbCl_3$ PNCs and TEM images of (b) $CsPbCl_3$ (c) Zn^{2+} added ($Zn(Ac)_2$ as Zn source) $CsPbCl_3$, (d) TMS-Cl added (triethylchlorosilane as Cl source) $CsPbCl_3$, and (e) both ($Zn(Ac)_2$ +TMS-Cl) co-added $CsPbCl_3$ PNCs.

The $Zn(Ac)_2$ (Zn to Pb ratio 1:1) alone doped $CsPbCl_3$ crystal lattice exhibited reduced PL emission and also redshifted compared to pristine $CsPbCl_3$ PNCs. When Zn ions were introduced, it is hard for them to enter into $CsPbCl_3$ crystal structure because of the rigid octahedron structure of Pb^{2+} surrounded by six Cl^- ions $[PbCl_6]^{4-}$ and may be restricted to surface confirming the difficulty in direct Zn to Pb cation exchange to proceed owing to the discrepancy in the bond dissociation energies. When TMS-Cl (1 mmol) alone was added to the $CsPbCl_3$ PNCs, the PL intensity has been enhanced with a blue shift which could be due to the suppression of formation of vacancies by additionally available monovalent chloride ions and consequently improved PL stability. However, the increase of additional chloride content alone in the host lattice may change its structural phase and also increase the bandgap making it undesirable for device fabrication. Thereafter, on combinedly doping $Zn(Ac)_2$ and TMS-Cl of 1 mmol each into to $CsPbCl_3$ NCs, a further increase in the PL intensity is observed. This is because the TMS-Cl promotes Cl^- ions to form $[ZnCl_6]^{4-}$ octahedra replacing $[PbCl_6]^{4-}$ in $CsPbCl_3$ structure by Cl^- to Cl^- anion exchange, favoring more Zn ions to substitute for Pb ions. Therefore incorporation of Zn^{2+} and Cl^- ions increased the PL intensity by relaxing the lattice relaxation and suppressing the formation energy of chlorine vacancies.[6,7] Recently, Mondal et al.,[8] reported that in $CdCl_2$-doped $CsPbCl_3$ PNCs, both Cd^{2+} and Cl^- have eliminated the halide vacancies and reduced the distortion in octahedral units. From our present analysis, it is realized that Zn^{2+} and Cl^- ions played a dominant role in relaxing the lattice strain suppressing the chlorine vacancies in PNCs. Figure S7(b-e) show the TEM images of pristine $CsPbCl_3$ PNCs, Zn^{2+} added ($Zn(Ac)_2$ as Zn source) $CsPbCl_3$, TMS-Cl added (trimethylchlorosilane as Cl source) $CsPbCl_3$, and both ($Zn(Ac)_2$ +TMS-Cl) co-added $CsPbCl_3$ PNCs. The $CsPbCl_3$ PNCs displayed well defined crystalline structure, Zn^{2+} ($Zn(Ac)_2$) doped $CsPbCl_3$ PNCs exhibited irregular shaped crystalline structure while TMS-Cl added $CsPbCl_3$ PNCs shown partially tetragonal and $Zn(Ac)_2$+TMS-Cl co-added $CsPbCl_3$ PNCs demonstrated a cubic structure (Figure S7(b-e))[6].

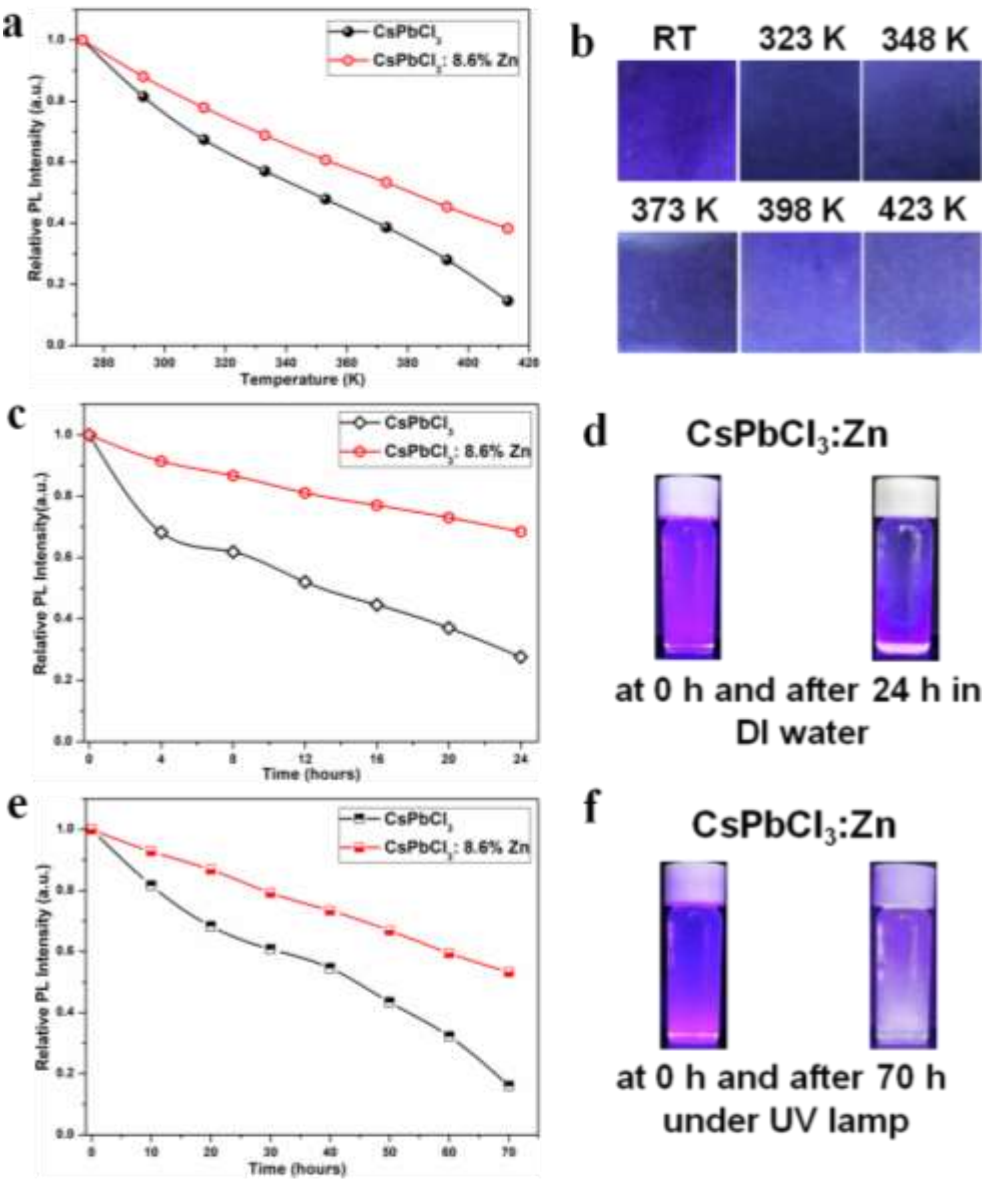

Figure S8. (a) Temperature-dependent integrated PL intensity for both pristine and Zn-doped $CsPbCl_3$ PNCs studied in the same temperature range, (b) Photographs of $CsPbCl_3$:8.6% Zn PNCs coated on the glass slide surface and annealed at different temperatures, (c) Relative PL intensity of both pristine and Zn-doped $CsPbCl_3$ PNCs and (d) photographs of Zn-doped PNCs immersed in DI water for 24 hours. (e) Relative PL intensity as a function of UV light irradiation time on $CsPbCl_3$, and $CsPbCl_3$:8.6% Zn, PNCs and (b) photographs of Zn-doped PNCs solution under UV lamp for 70 hours.

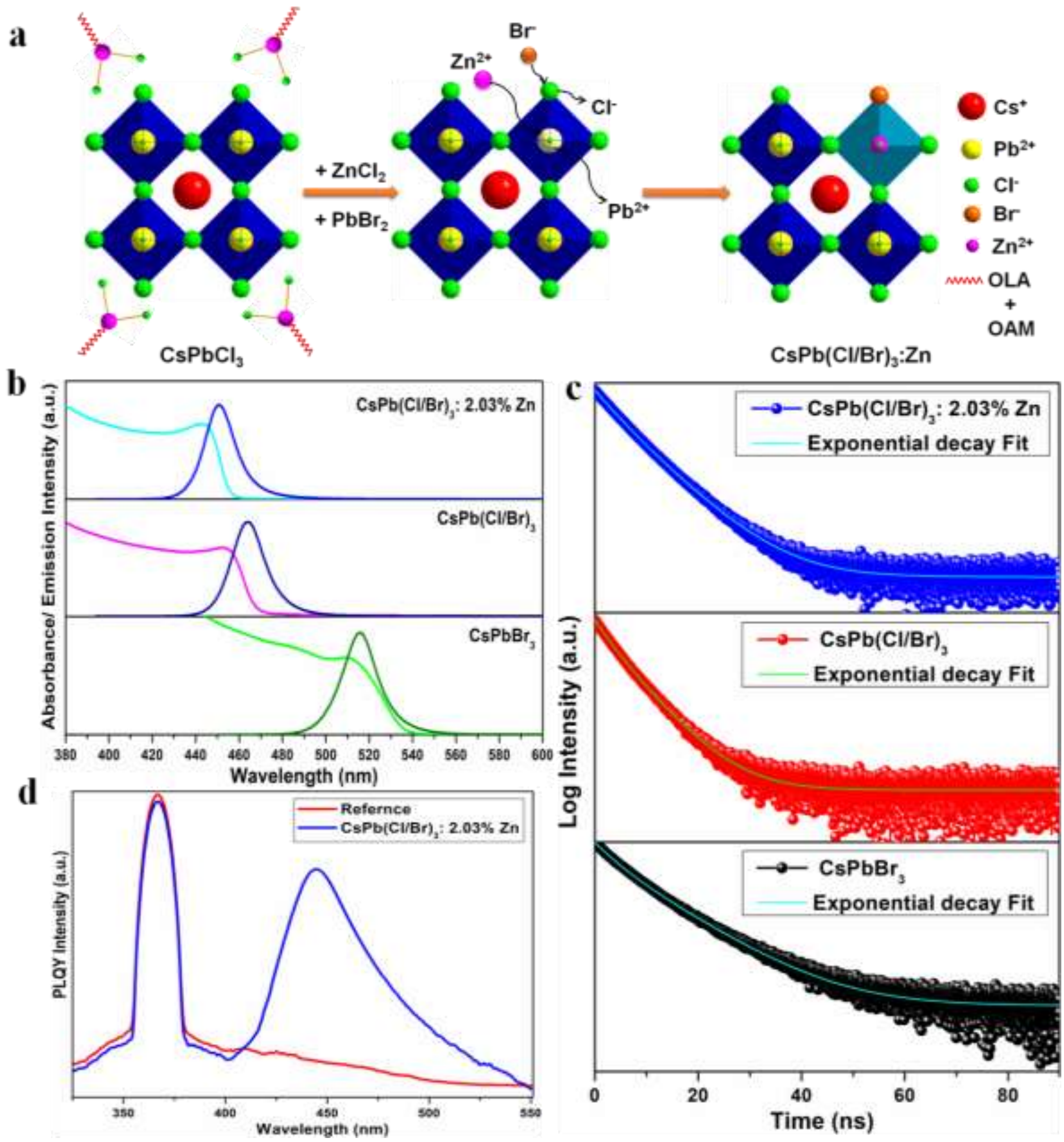

Figure S9. (a) Divalent cation (Zn^{2+}) and monovalent halide (Cl-to-Br) or anion exchange process in $CsPbCl_3$ perovskite NCs. (b) Optical absorption and photoluminescence spectra and (c) Lifetime decay curves of pristine $CsPbBr_3$, $CsPb(Cl/Br)_3$ and $CsPb(Cl/Br)_3$:2.03%Zn PNCs. Inset figures show the images of doped and undoped PNCs dispersed in n-hexane solution under 365 nm (UV) light irradiation. (d) PLQY measurement of $CsPb(Cl/Br)_3$: 2.03% Zn PNCs.

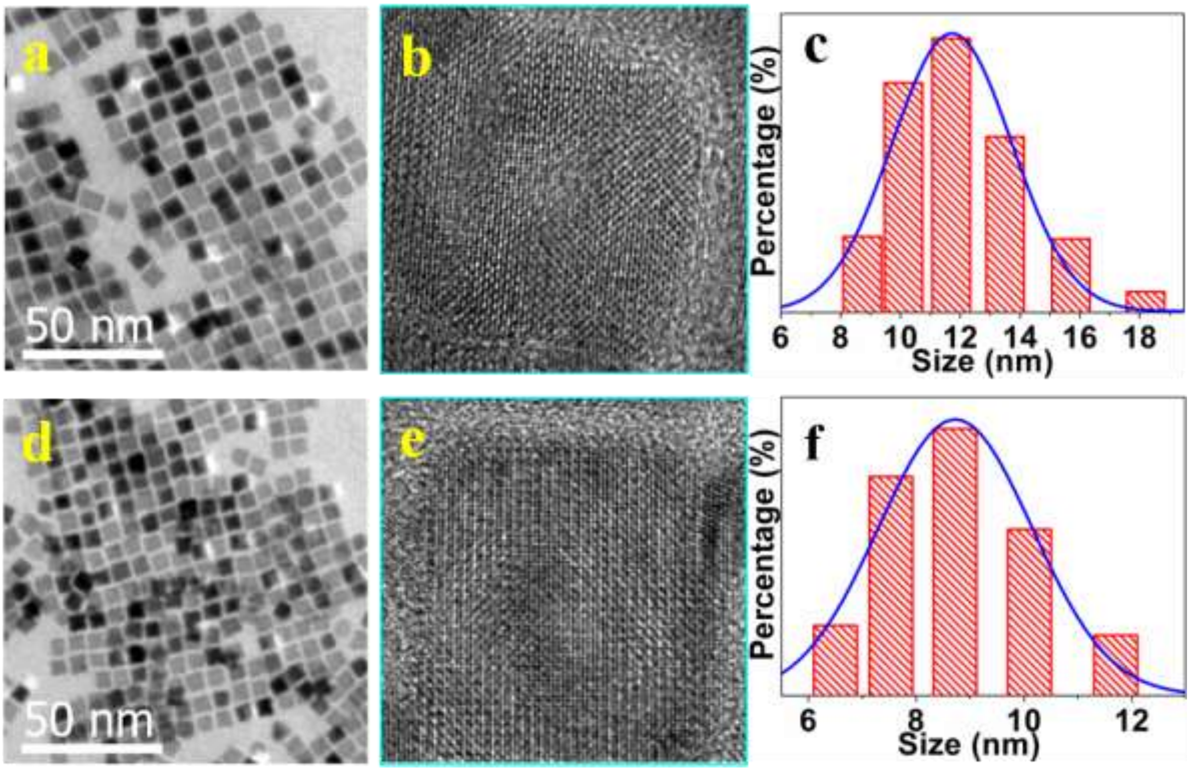

Figure S10. (a-c) and (d-f) represents the TEM, HR-TEM images and their corresponding particle distribution histograms displaying avg edge length of $CsPb(Cl/Br)_3$, $CsPb(Cl/Br)_3$: 2.03% Zn PNCs as 11.72 nm and 8.8 nm, respectively.

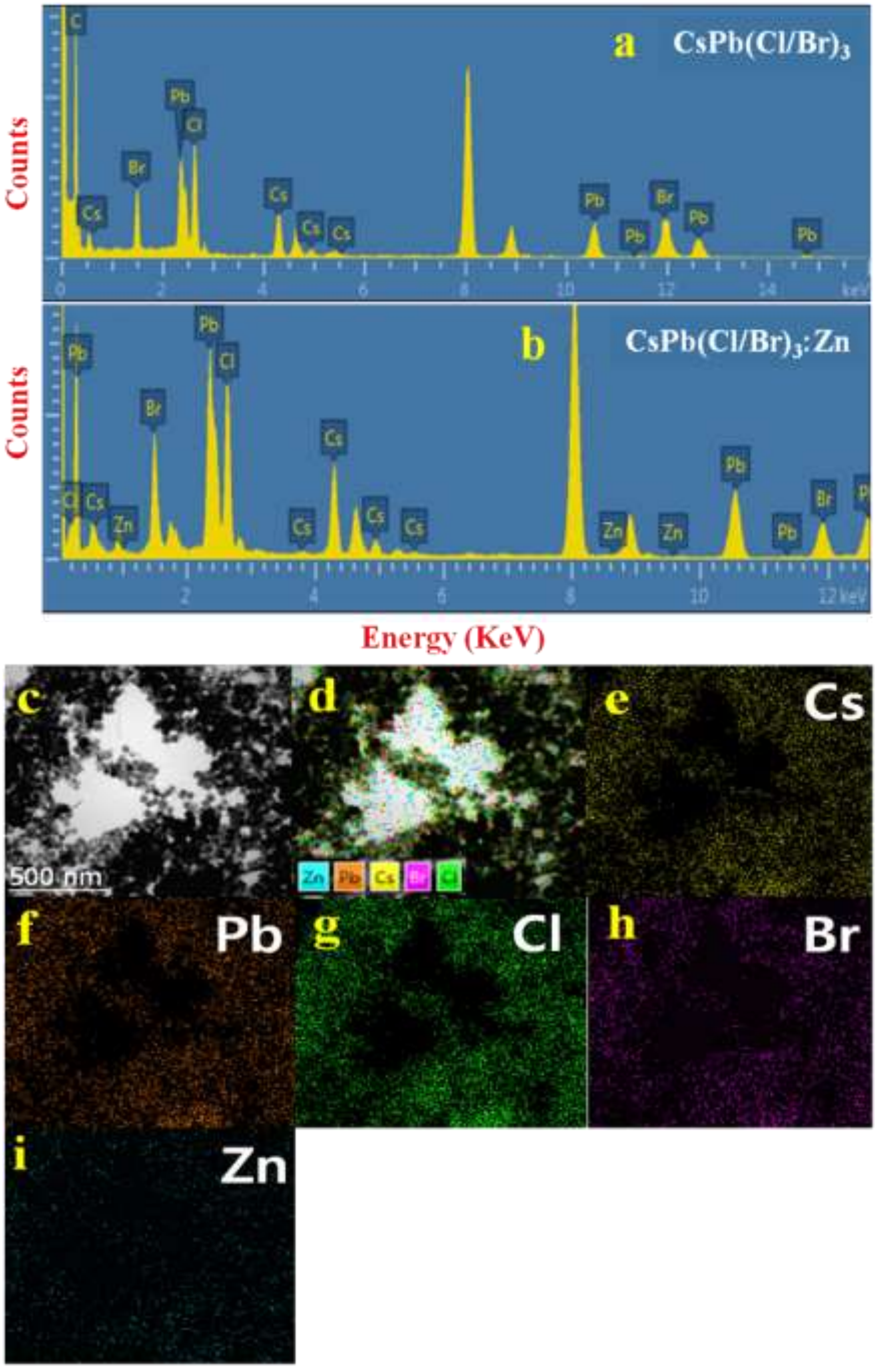

Figure S11. (a-g) Elemental signal (EDS) profiles of (a) $CsPb(Cl/Br)_3$, (b) $CsPb(Cl/Br)_3$: Zn (c-i) elemental composition (mapping) images of Cs, Pb, Cl, Br and Zn in $CsPb(Cl/Br)_3$:Zn PNCs.

Table S5. PL peak position, FWHM, average lifetimes τ_{avg} of fitted PL decay curves, PLQYs, radiative (τ_r) and non-radiative (τ_{nr}) decay rates of $CsPbX_3$ and $CsPbX_3$: 2.03% Zn (X = Cl, and Cl/Br).

Nanocrystal composition	PL peak position (nm)	FWHM (nm)	τ_{avg} (ns)	PLQY (%)	τ_r (ns^{-1})	τ_{nr} (ns^{-1})
$CsPbCl_3$	409	10.11	1.35	3.2	0.023	0.71
$CsPbCl_3$: 8.6% Zn	408	14.13	4.62	88.7	0.191	0.025
$CsPb(Cl/Br)_3$	464	18.48	2.56	25	0.098	0.902
$CsPb(Cl/Br)_3$: 2.03% Zn	451	16.06	9.1	92	0.101	0.0088
$CsPbBr_3$	518	21.13	7.9	85	0.1075	0.019

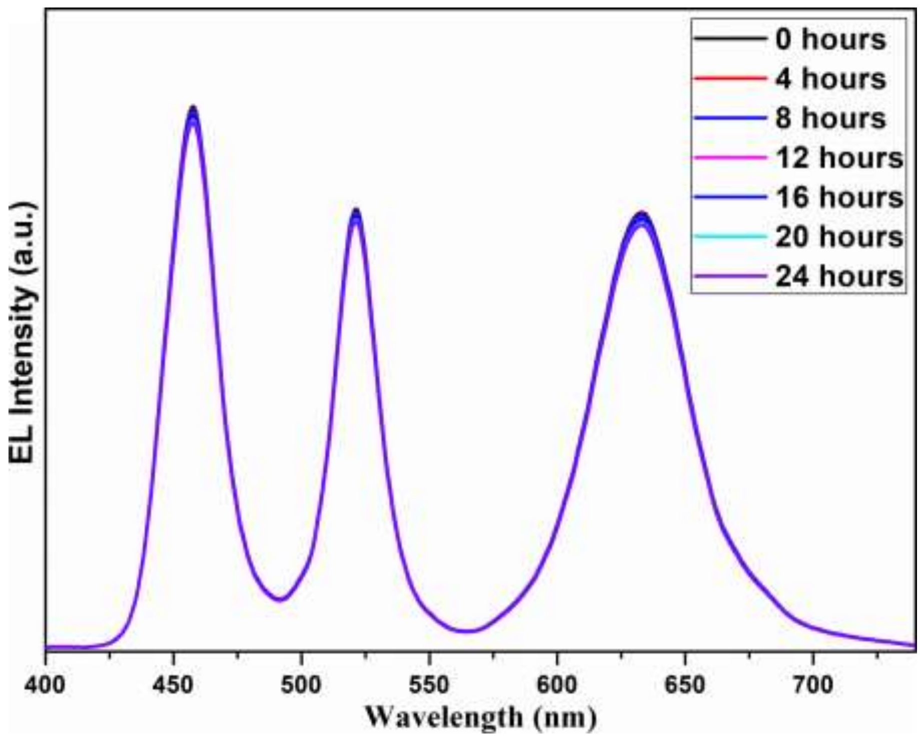

Figure S12. Electroluminescence spectra of W-LED operating at different time intervals (0-24 hr).

Table S6. Summary of comparison of CIE coordinates, Luminous efficiency (LE), color temperature (CCT), colour rendering index (CRI), and wide color gamut (NTSC %) for the constructed w-LED using Zn-CsPb(Cl/Br)+$CsPbBr_3$+$CsPb(Br/I)_3$@PMMA with other designed perovskite w-LED systems.

Constructed w-LED system	CIE w-light coordinates	LE (lm/W)	CCT (K)	CRI	Color gamut (NTSC %)	Refer-ences
Zn-CsPb(Cl/Br) @PMMA	(0.321, 0.296)	67.5	6285	86.3	118	*Present work*
Mn-$CsPbCl_3$@SiO_2	(0.392, 0.401)	77.59	5128	88	-	*Ref. 9*
Mn-$CsPb(Cl/Br)_3$ @SiO_2	(0.320, 0.391)	40	5942	84.6	-	*Ref. 10*
$CsPbX_3$QDs/PDMS	(0.32, 0.33)	40.3	6113	-	-	*Ref. 11*
Al-$CsPbX_3$ NCs	(0.32,0.34)	87	6073	-	116	*Ref. 12*
$CsPbBr_3$/PMMA	(0.341,0.332)	-	-	89.2	105	*Ref. 13*
$CsPbBr_3$-SiO_2	(0.329,0.359)	35.4	5623	-	127	*Ref. 14*
$CsPb(Br/I)_3$-glass	(0.346,0.347)	69.8	4947	-	100.1	*Ref. 15*

References

(1) Yong, Z.-J.; Guo, S.-Q.; Ma, J.-P.; Zhang, J.-Y.; Li, Z.-Y.; Chen, Y.-M.; Zhang, B.-B.; Zhou, Y.; Shu, J.; Gu, J.-L.; Zheng, L.-R.; Bakr, O. M.; Sun, H.-T. Doping-Enhanced Short-Range Order of Perovskite Nanocrystals for Near-Unity Violet Luminescence Quantum Yield. *J. Am. Chem. Soc.* **2018**, 140, 9942–9951.

(2) Mondal, N.; De, A.; Samanta, A. Achieving Near-Unity Photoluminescence Efficiency for Blue-Violet-Emitting Perovskite Nanocrystals. *ACS Energy Lett.* **2019**, 4, 32–39.

(3) Chen, J.-K.; Ma, J.-P.; Guo, S.-Q.; Chen, Y.-M.; Zhao, Q.; Zhang, B.-B.; Li, Z.-Y.; Zhou, Y., Hou, J.; Kuroiwa, Y.; Moriyoshi, C.; Bakr, O. M.; Zhang, J.; Sun, H.-T. High-Efficiency Violet-Emitting All-Inorganic Perovskite Nanocrystals Enabled by Alkaline-

Earth Metal Passivation. *Chem. Mater.* **2019**, 31, 3974−3983.

(4) De, A.; Das, S.; Mondal, N.; Samanta, A. Highly Luminescent Violet- and Blue-Emitting Stable Perovskite Nanocrystals. *ACS Materials Lett*. **2019**, 1, 116–122.

(5) Rana, P. J. T.; Swetha, T.; Mandal, H.; Saeki, A.; Bangal, P. R.; Singh, S. P. Energy Transfer Dynamics of Highly Stable Fe^{3+} Doped $CsPbCl_3$ Perovskite Nanocrystals with Dual-Color Emission, *J. Phys. Chem. C* **2019**, 123, 17026−17034.

(6) Zhou, S.; Zhu, Y.; Zhong J.; Tian, F.; Huang H.; Chen, J.; Chen, D. Chlorine-Additive-PromotedIncorporation of Mn^{2+} Dopants into $CsPbCl_3$ Perovskite Nanocrystals. *Nanoscale* **2019**, 11, 12465.

(7) Saidaminov, M.; Kim, J.; Jain, A.; Quintero-Bermudez, R.; Tan, H.; Long, G.; Tan, F.; Johnston, A.; Zhao, Y.; Voznyv, O.; Sargent, E.H. Suppression of Atoic Vacancies via Incorportion of Isovalent Small Ions to Increase the Stability of Halide Perovskite Solar Cells in Ambient Air. *Nature Energy* **2018**, 3, 648–654.

(8) Mondal, N.; De, A.; Samanta, A. Achieving Near-Unity Photoluminescence Efficiency for Blue-Violet-Emitting Perovskite Nanocrystals. *ACS Energy Lett.* **2019**, 4, 32–39.

(9) Chen, W. W.; Shi, T.; Du, J.; Zang, Z.; Yao, Z.; Li, M.; Sun, K.; Hu, W.; Leng, Y.; Tang, X. Highly Stable Silica-Wrapped Mn-Doped $CsPbCl_3$ Quantum Dots for Bright White Light-Emitting Devices. *ACS Appl. Mater. Interfaces* **2018**, 10, 43978–43986.

(10) Chen, D.; Fang, G.; Chen, X. Silica-Coated Mn-Doped $CsPb(Cl/Br)_3$ Inorganic Perovskite Quantum Dots: Exciton-to-Mn Energy Transfer and Blue-Excitable Solid-State Lighting. *ACS Appl. Mater. Interfaces* **2017**, 9, 40477–40487.

(11) Zhihai, W.; Jiao, W.; Yanni, S.; Jun, W.; Yafei, H.; Pan, W.; Nengping, W; Zhenfu, Z. Air-stable all-inorganic perovskite quantum dot inks for multicolor patterns and white

LEDs. *J. Mater. Sci.* **2019**, 54, 6917–6929.

(12) Liu, M.; Zhong, G.; Yin, Y.; Miao, J.; Li, K.; Wang, C.; Xu, X.; Shen, C.; Meng, H. Aluminum-Doped Cesium Lead Bromide Perovskite Nanocrystals with Stable Blue Photoluminescence Used for Display Backlight. *Adv. Sci.* **2017**, 1700335.

(13) Ma, K.; Du, X.-Y.; Zhang, Y.-W.; Chen, S. In situ Fabrication of Halide Perovskite Nanocrystals Embedded in Polymer Composites via Microfluidic Spinning Microreactors. *J. Mater. Chem.* C **2017**, 5, 9398–9404.

(14) Park, D. H.; Han, J. S.; Kim, W.; Jang, H. S. Facile Synthesis of Thermally Stable $CsPbBr_3$ Perovskite Quantum Dot-Inorganic SiO_2 Composites and Their Application to White Light-Emitting Diodes with Wide Color Gamut. *Dyes and Pigments* **2018,** 149, 246–252.

(15) Xiang, X.; Lin, H.; Xu, J.; Cheng, Y.; Wang, C.; Zhang, L.; Wang, Y. $CsPb(Br,I)_3$ Embedded Glass: Fabrication, Tunable Luminescence, Improved Stability and Wide-Color Gamut LCD Application. *Chem. Eng. J.* **2019**, 378, 122255.